

Microwave-stimulated superconductivity due to presence of vortices

Antonio Lara¹, Farkhad G. Aliev^{1,*}, Alejandro V. Silhanek², and Victor V. Moshchalkov³

¹*Dpto. Física Materia Condensada, Instituto Nicols Cabrera (INC) and Condensed Matter Physics Institute (IFIMAC),*

Universidad Autónoma de Madrid, 28049, Madrid, Spain

²*INPAC- Katholieke Universiteit Leuven, Celestijnenlaan 200D,*

B3001, Leuven, Belgium and Departement de Physique,

Université de Liège, B-4000 Sart Tilman, Belgium and

³*INPAC- Katholieke Universiteit Leuven, Celestijnenlaan 200D, B3001, Leuven, Belgium*

(Dated: November 13, 2021)

arXiv:1503.01610v2 [cond-mat.supr-con] 9 Mar 2015

* Corresponding author: farkhad.aliev@uam.es

The response of superconducting devices to electromagnetic radiation is a core concept implemented in diverse applications, ranging from the currently used voltage standard to single photon detectors in astronomy. Surprisingly, a sufficiently high power subgap radiation may stimulate superconductivity itself. The possibility of stimulating type II superconductors, in which the radiation may interact also with vortex cores, remains however unclear. Here we report on superconductivity enhanced by GHz radiation in type II superconducting Pb films in the presence of vortices. The stimulation effect is more clearly observed in the upper critical field and less pronounced in the critical temperature. The magnetic field dependence of the vortex related microwave losses in a film with periodic pinning reveals a reduced dissipation of mobile vortices in the stimulated regime due to a reduction of the core size. Results of numerical simulations support the validity of this conclusion. Our findings may have intriguing connections with holographic superconductors in which the possibility of stimulation is under current debate.

Microwave (mw) irradiation has been used to control the quantum properties of different systems, from supercurrents in superconductors to mechanical oscillators [1–4]. Using nonequilibrium pumping for cooling is currently a hot topic [5, 6]. In 1966 microwave stimulated superconductivity (MSSC) was discovered [7] in superconducting bridges and later confirmed for different type I superconducting systems such as films [8, 9], tunnel junctions [10] or cylinders [11, 12]. This counterintuitive effect was explained by Eliashberg [7] as a consequence of an irradiation-induced redistribution of quasiparticles away from the gap edge. Very recently MSSC has been observed in transient regimes (on ps time scales) in NbN films [14] and was demonstrated to improve the quality factor of superconducting mw resonators [15].

In type II superconductors with magnetic field penetrating in form of quantized flux (vortices) [16], the reduced inelastic relaxation time could suppress or modify some signatures of MSSC. A renewed interest in the type II SCs is related with the proposal of holographic superconductors (HS) [17], mapping solutions of astrophysics problems to scalar condensates. Just like as type II SCs in solid state, HSs can exhibit vortex configurations [18] and can be phenomenologically described by the time dependent Ginzburg-Landau equation (TDGL) [19] in the proximity of the critical temperature. The possibility of stimulated SC in the HSs is under current debate [20, 21]. Clearly, the experimental verification of stimulated superconductivity in type II SCs in the vortex state could therefore have important implications both inside and outside condensed matter physics community, paving the way for further progress in modelling physics of black holes and gravity through HSs.

A periodic mw pump of sufficient amplitude induces the motion of vortices that results in dissipation [22–25]. Though dynamics of vortices was extensively addressed [26], the possibility of MSSC in the vortex state is not fully understood. One can speculate that the energy balance in microwave-driven vortices should depend on a competition between friction-induced heating of quasiparticles in the vortex cores [27–29] and energy pumping outside the core at large vortex velocities [30]. However, the full picture of nonlinear electromagnetic response of the vortex matter in the proximity to the critical temperature remains unsettled.

Our paper reports on broadband nonlinear response to mw radiation in the GHz range in type II superconducting

Pb films. We observe experimentally MSSC in an enhancement of the critical temperature, while much larger effects are seen in the second critical field. In order to investigate stimulation under varying pinning strength (i.e. vortex motion amplitude), we have carried detailed studies of MSSC in the Pb films with periodic pinning centers (Pb-PCC) and with applied DC field inclined about 4° off the film plane. Such configuration has been chosen because the most pronounced effect has been observed with it. Besides, the small perpendicular field component H_\perp creates vortices, permitting us, by properly choosing the magnetic field intensity, to achieve the situations where the number of vortices is an integer multiple of the number of pinning centers (matching conditions). In that case, the vortex lattice rearranges itself in a specially stable manner, and vortex motion becomes restricted. Therefore, the commensurability between the vortex lattice and the periodic pinning centers facilitates the investigation of the complex vortex dynamics under periodically varying pinning conditions. The experiments unambiguously reveal a reduction of the dissipation of microwave driven mobile superconducting vortices at moderate frequencies and powers. Supported by TDGL simulations, we relate this unexpected behaviour to the reduction of the vortex core size at large vortex velocities, predicted by Larkin and Ovchinnikov (LO) [30] and seen indirectly when the flux is driven with a DC current [31].

RESULTS

Stimulation of critical temperature and upper critical field. A description of the samples and measurement details are provided in the Methods section and in the Supplementary material. Figure 1b shows the real and imaginary parts of the microwave permeability parameter U , defined in the Methods section, measured in Pb-PPC at small mw powers. Measurements are done in a temperature (T) sweep for different magnetic fields, at a fixed frequency (f) and are in accordance with the Coffey-Clem model [33]. The dependence of the response on the mw power (P) for the same Pb-PPC sample is seen in the contour plot for U' in the plane $P - T$ for magnetic field $H = 0$ and $f = 6$ GHz, (Fig. 1c). To characterize the shift of the transition as a function of P , we introduce an effective critical temperature, T_c^* , (Supplementary Fig. A3), determined with an error around 1 mK. Figure 1d presents a 3D plot of T_c^* in the coordinates $P - H$ in the Pb-PPC at $f = 6$ GHz. One observes a non-monotonic dependence of $T_c^*(P)$, increasing at small P and decreasing at large P . Though the T_c^* does not have the meaning of critical temperature of the superconducting transition, the observed increase of T_c^* can be interpreted as an indication of MSSC.

To investigate the nonlinear response in the vortex state as a function of pinning strength, we have carried out measurements of U' and U'' as functions of H , P , f and T in Pb-PPC. Figure 2a shows a 3D plot of U' for the Pb-PCC sample at $T = 7.19$ K in the coordinates $H - P$. Dark red tones correspond to the normal state. As H is lowered, the samples become superconducting and the magnetic permeability changes in agreement with expectations [33]. Figure 2b shows a typical set of cross-sections of U' at fixed magnetic fields. While mw power above 5 dBm destroys superconductivity, for intermediate values the superconducting response is the most intense. We will refer to the applied P that yields the strongest superconducting response as “optimum power” (P_O). The dashed line indicates how P_O changes with H . The response (inset of Fig. 2b) shows directly transition between linear to nonlinear vortex response regimes. At lowest powers it flattens and is noisier, since the relative noise is larger compared to the weaker signal received in port 2 of the network analyzer.

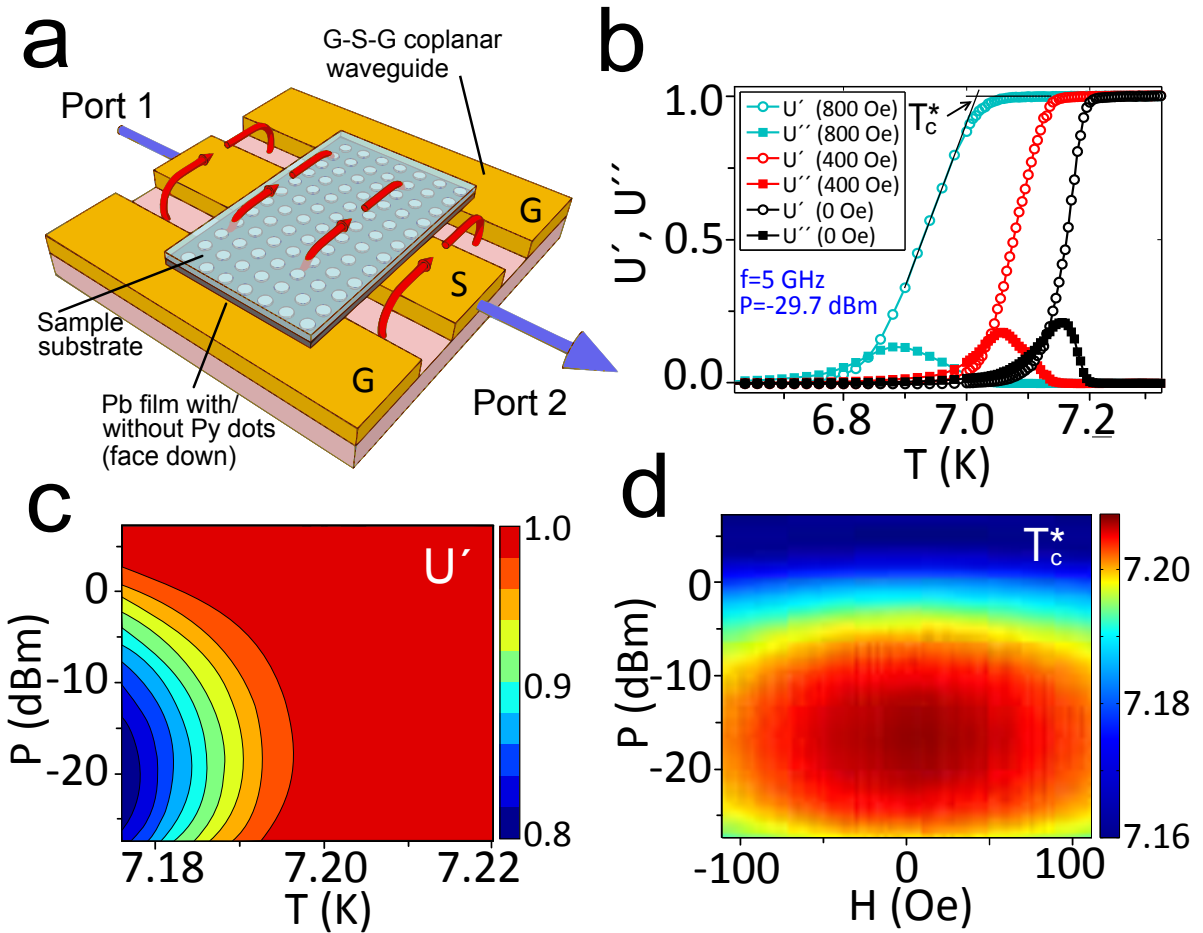


FIG. 1. Sketch of the sample and effect of stimulation on critical temperature. a) Sketch of the sample placed face down on the ground-signal-ground (G-S-G) coplanar waveguide (CPW). Red arrows represent the magnetic field generated by the CPW. b) Measurements of U' and U'' at different fields. c) Contour plot of U' versus microwave power and temperature, measured at $f = 6$ GHz. d) T_c^* in the field range from $H = -120$ Oe to $H = 120$ Oe. All data correspond to the Pb-PPC sample.

Similarly to T_c^* , we introduce an effective critical magnetic field, H_{c2}^* . Figure 2c shows a plot of $H_{c2}^*(P, T)$ in the Pb-PPC sample (see Supplementary material for the method of finding H_{c2}^* , and the results for the plain film). For each temperature, H_{c2}^* has been normalized by its value at the lowest P , so relative values of H_{c2}^* can be compared. As $T \rightarrow T_c$, the relative increase of H_{c2}^* under mw at $P = P_O$ becomes larger. Figure 2d compares the normalized H_{c2}^* as a function of reduced temperature in both types of samples (with and without pinning centers), showing that MSSC effects in H_{c2}^* are stronger in the Pb-PPC sample.

Figure 3a shows that $P = P_O$ increases with mw frequency with a maximum value that saturates around 15 GHz. These frequencies are well below those corresponding to the superconducting gap.

Reduced dissipation of microwave driven mobile vortex. The changes in P_O indicate that the “cooling” effectiveness of mw radiation depends on the pinning strength through the applied field which changes the number of vortices per pinning center and correspondingly their mobility. In Fig. 3b this fact is exposed for $f = 6$ GHz, at different values of T . Solid lines show P_O vs. magnetic field with matching conditions indicated by vertical dotted

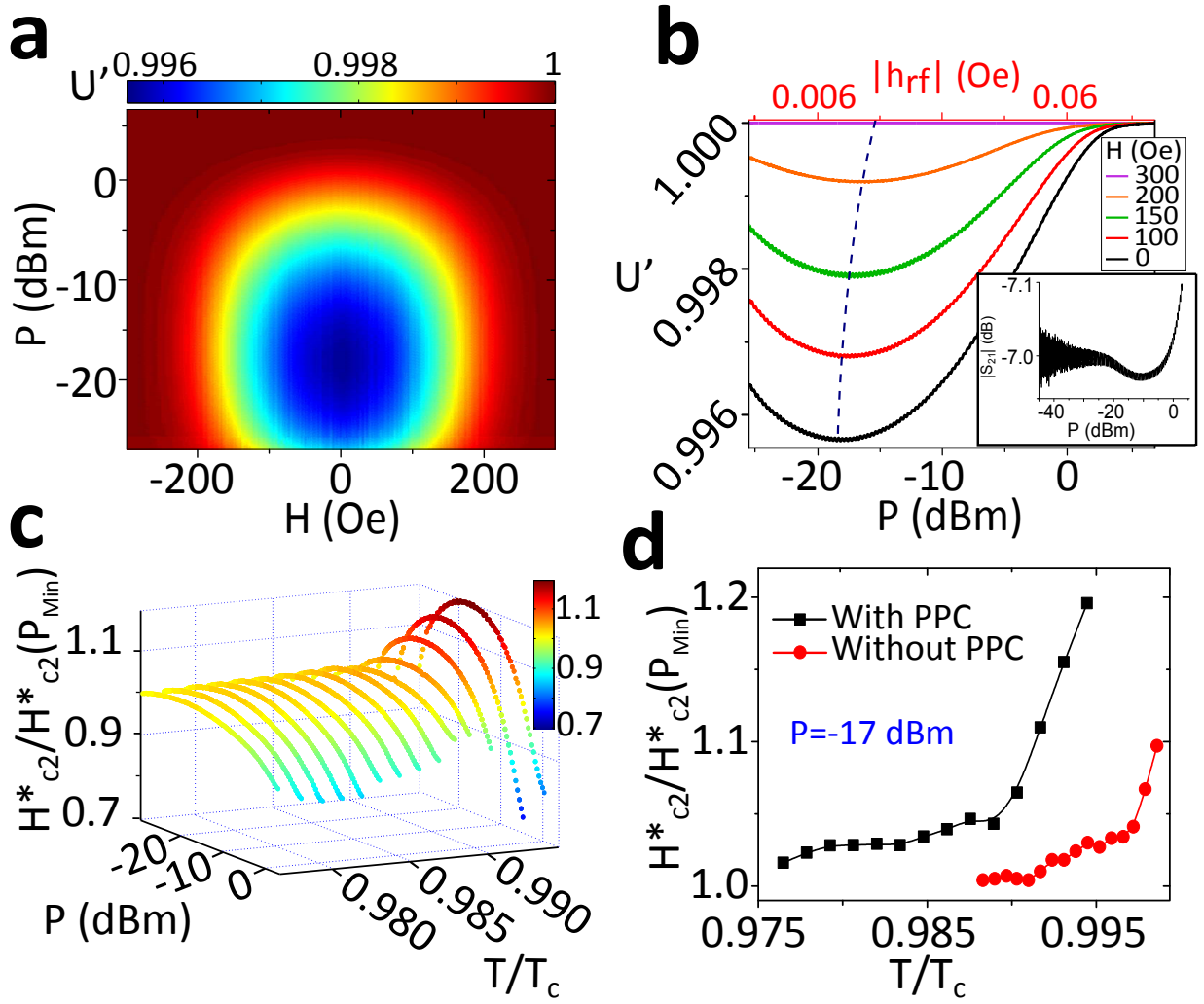


FIG. 2. Effect of stimulation on the upper critical field. a) Real part of the microwave permeability at $T = 7.19K$, as a function of applied field and microwave power. b) Cross sections of panel a) at fixed fields. The dashed line indicates optimum power. The inset shows a $|S_{21}|$ trace in a broader power range, at $H = 0$ Oe, $f = 4$ GHz and $T/T_c = 0.991$. c) H_{c2}^* for different T and P for the Pb-PPC sample. Values are normalized at each T by the values of H_{c2}^* at the minimum power. d) Comparison of normalized H_{c2}^* for each sample.

lines. Red circles represent a typical measurement of $U'(f, P, H)$ at fixed values of f and P , in which the same matching anomalies appear in the mw permeability. The lowest value of P_O for every temperature is found always at zero field, and decreases locally in matching conditions. This hints the relevance of the vortex mobility for the value of P_O : the enhanced vortex mobility out of matching conditions provides relatively larger (respect to matching) P_O values and correspondingly larger "cooling" efficiency.

This counterintuitive result has been corroborated through a set of independent experiments investigating the H and P dependencies of U'' . At low f , when MSSC is not yet pronounced, the dissipation (U'') at matching conditions shows (as expected) dips in a broad range of P (Supplementary Fig. A.7). However, for higher f the dips of losses at matching conditions convert into peaks. The same effect can be observed as a function of power, in Fig. 3c.

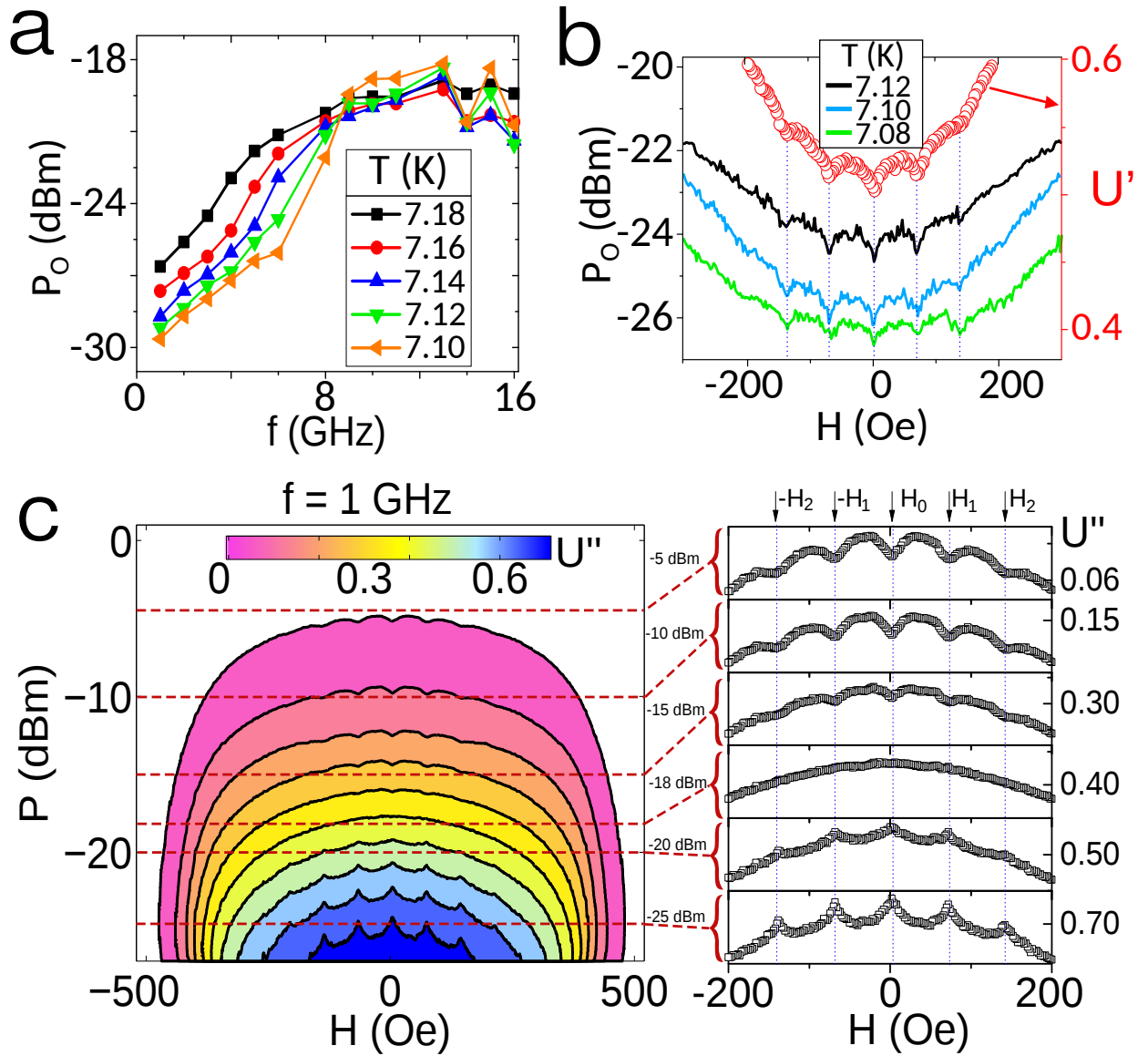


FIG. 3. Nonlinear response of vortex losses at matching conditions. a) P_O versus f . b) Lines represent optimum power (P_O) as a function of applied field at $f = 6$ GHz. Red circles (right axis) represent U' . Minima in P_O appear at matching fields. U'' in a power sweep is shown for $f = 1$ GHz in panel c). The right part are cross sections at fixed powers. All panels correspond to the Pb-PPC sample.

In other words, *vortices moving with higher average velocities out of matching conditions manage to dissipate less than pinned in matching conditions*. These observations indicate a qualitative change in the microwave response of superconducting vortices at high *mw* frequencies.

DISCUSSION

Mechanism of nonlinear vortex response and modelling. Mechanisms of nonlinear response of vortices to microwave radiation are far from being fully understood. LO theory [30] predicts a nonlinear response at sufficiently

large electric fields, that induces a high speed DC motion of the vortices. If their speed exceeds some critical value, v_c , much lower than the critical velocity for breaking Cooper pairs, the current decreases with increasing voltage. This is a consequence of an electronic instability of the non-equilibrium distribution of quasiparticles at high velocities, leading to a reduction of the vortex core size. A further increase of vortex velocity leads to an abrupt switching into a state with higher electric resistivity. On the other hand, the nonequilibrium quasiparticle distribution close to the energy gap where the density of states is maximal can cause stimulation of superconductivity [7]. One can anticipate an interplay between the above mechanisms in a mixed state of mw driven type-II superconductors. However, we are not aware of a theory quantitatively interpreting our experimental results.

To understand the nonlinear response of mw driven vortices we have simulated the ac response of vortices using the time dependent Ginzburg-Landau equations (see Supplementary material for details). The time derivative of the order parameter modulus $|\Psi|$ shows that vortices oscillate about their equilibrium positions, especially at lower frequencies, when they are able to follow the external ac field without delay (Supplementary Fig. A.9 b). As the ac field amplitude increases (which is equivalent to increasing the mw power of our measurements) the order parameter oscillates throughout the entire sample, being weaker at the maxima of amplitude of mw field h_{rf} , as expected. This effect is specially pronounced in the outer part of vortex cores, as can be seen in Fig. 4b,c. When one compares the radius of a vortex (at a given value of, for example, $|\Psi| = 0.5$, see Fig. 4c) for different moments of an oscillation period, vortices are narrower at zero ac field amplitude than at its maximum ac . As happens in vortex cores displacement, the higher the frequency of the ac field, the more difficult is for a vortex core radius to change size (see Fig. 4d). A transition from linear to nonlinear response regimes is observed, *leading to a substantial reduction of the average vortex size* at high mw drives as a function of f . The reason for the different ranges of frequencies considered in the experiment and simulation are commented in the methods section.

The oscillations of the vortex core size under mw radiation are always present, and more notorious for higher ac field amplitudes, which is in qualitative agreement with the DC model by LO [30]. The above confirmation of LO-type mechanism in ac conditions agrees with simulations of DC driven vortices [34] and does not exclude electron overheating in the vortex core as an additional factor contributing anomalous velocity dependence of vortex viscosity [29].

The vortex velocity can be limited by the critical value v_c for the LO instability [30, 31, 35]. Assuming that the maximum mw -induced shift of a vortex is limited by the inter-dot distance $a \lesssim (1 - 1.5) \mu\text{m}$ and that the dependence of P_O on f starts to saturate at $f \gtrsim f_{\text{sat}} \sim 10 \text{ GHz}$ we estimate the geometrically restricted maximal vortex velocity as $v_{\text{max}} = f_{\text{sat}} \cdot a \approx 6 - 10 \text{ km/s}$. This is 2-3 times larger than the values of v_c reported for Nb and high- T_c superconducting films [25, 36].

Summary and conclusions. The experimental observation of stimulated superconductivity in type II superconductors has been used to quantify relative changes in vortex dissipation as a function of mobility (pinning). At high enough mw power and/or low enough mw frequencies (Fig. 3c) when MSSC is not effective, the vortex matching effects are clearly observed as periodic *dips in the mw losses* when $H_{\perp} = n\Phi_0/a^2$ (n is an integer number and Φ_0 the magnetic flux quantum). In contrast to that, in a broad range of mw powers (sufficiently below limiting values

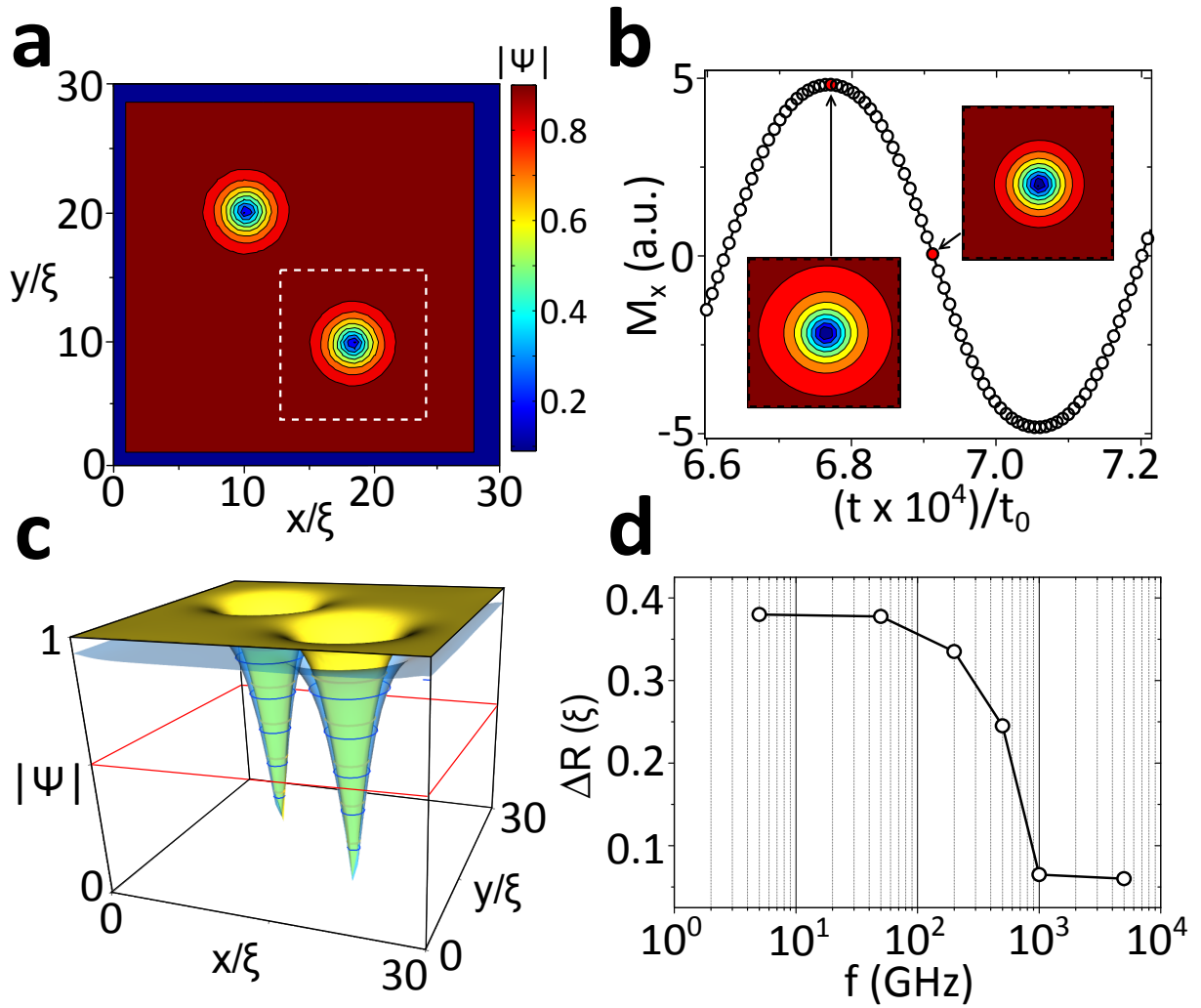


FIG. 4. Time dependent Ginzburg-Landau simulations. a) Contour plot of $|\Psi|$ in a square sample, with $H_{DC} = 0.02H_{c2}$ perpendicular to the sample, after applying $H_{DC} = 0.8H_{c2}$ and slowly reducing it. Two vortices are isolated. b) Oscillation of M_x (component of magnetization in the direction of the ac field, in arbitrary units) as a function of time, following the ac field at 5 GHz. Snapshots of the area marked by dashed white lines in panel a) show the different size of vortices at times separated by $1/4$ of a period. c) $|\Psi|$ at the whole sample for the two cases considered in b). Yellow surface corresponds to minimum and blue to maximum of $|H_{DC}|$. d) Change of vortex radius (taken at $|\Psi|=0.5$, marked by red line in panel c) as a function of frequency in an oscillation period. At high frequencies the vortices cannot follow the external field and their shape and position almost don't change

which heat the sample) and at high enough frequencies (above about 0.6 GHz) mobile (off-matching) vortices dissipate less than pinned vortices. One clearly observes *peaks in the vortex dissipation* in matching conditions. The higher the frequency, the broader the *mw* power range where matching anomalies are seen as peaks in losses. Microwave stimulation changes from dips at matching fields at the lowest frequencies to peaks at frequencies exceeding a few GHz, in agreement with TDGL simulations, that indicate a transition to a nonlinear regime when mobile (interstitial) vortices dissipate less than pinned ones. The observed effects (transition from peaks to dips) remain qualitatively

unchanged for the range up to 3 vortices per pinning center, meaning that intervortex interaction has a weak influence on our results. The supplementary video 1 shows a simulation of the vortex response to a mw magnetic field. One clearly observes the changes of the vortex core radius and (through differential analysis of the modulus of the order parameter) the vortices motion. We find vortex deformation to be minimum because its displacement at mw frequencies is small in comparison with radius oscillations.

We point out that stray fields of Py dots do not play an essential role for the effects we observe. Unlike previous simulations [37], our dots are in the magnetic vortex state with minimum stray fields [38] and with ferromagnetic resonance (FMR) suppressed [39], i.e., the dots are not saturated. Besides, there should be a strong structural pinning profile due to the fact that the SC film covers the array of dots and not vice versa as in [37]. A qualitative similarity in the microwave losses measured with perpendicular or with inclined nearly parallel magnetic fields (Supplementary Fig. A.8) further confirms that the observed effects are not induced by the presence of an in-plane component of magnetic field.

In conclusion, we have observed experimental signatures of stimulated superconductivity in type II superconductors in the vortex state including an enhancement of the upper critical fields and a somewhat less noticeable increase of the critical temperature. Moreover, we have found experimentally and supported by simulations the unique fingerprint of MSSC in vortex dynamics -the reduced dissipation of microwave driven vortices due to a reduction of the vortex core size. Besides significance for condensed matter physics, our results may have implications for the current controversy on the possibility of stimulated superconductivity in holographic superconductors [20, 21].

METHODS

We investigated two types of samples: plain 60 nm thick Pb films ($T_c \simeq 7.2\text{K}$) and 60 nm thick Pb films deposited over a square array of periodic pinning centers (Pb-PPC), consisting of circular Py dots (see Supplementary material for further details). All figures (except Fig. 2d and Supplementary Fig. A.5) refer to the Pb-PPC sample.

The broadband measurements were done with a Vector Network Analyzer (VNA) connected to a coplanar waveguide (CPW) situated inside a cryostat with a superconducting magnet (see Supplementary material for details). The VNA signal excites the sample, placed on the CPW (Fig. 1a). The complex mw permeability, $U \equiv U' + iU''$, is determined as the VNA transmission parameter S_{21} , dependent on microwave power (P), frequency (f), temperature (T) and magnetic field (H), normalized by S_{21} at a reference H or T , in the normal state (Supplementary material for more details). Experimental figures corresponds to the estimated values of power waves travelling through the waveguide, but not absorbed by the vortex system.

To understand better the individual behavior of superconducting vortices under the influence of an in plane ac magnetic field, we have simulated the TDGL equation in 3D. Simulations allow to include a DC field perpendicular to the film to create vortices, and a sinusoidal field parallel to the plane that represents the mw field generated by the CPW. Both field components are introduced through the appropriate boundary conditions (see Supplementary material). Our simulations are based on the finite difference approach used several times in the past in 2D (see for

example [8]). The Ginzburg-Landau parameter used is $\kappa = 2$. The temperature has been fixed far from $T_c = 7.2K$ ($T = 4K$) because vortices are better observed, being the results obtained still valid (although less visible) at higher temperatures. A mismatch between the frequency range presented in the measurements and that of the simulations is due to the absence of precise knowledge of the characteristic time scales of the normal and superconducting parts of the GL simulation. We use our simulation just for qualitative confirmation of existence of LO mechanism for the microwave driven vortex. Future work could also try to analyze numerically possible coupled magnetic dot-superconducting vortex dynamics. This task, however, presents great challenge because of the need to include dynamics of magnetic pinning centers.

-
- [1] Lindner, N. H., Refael, G. & Galitski, V. Floquet topological insulator in semiconductor quantum wells. *Nature Phys.* **7**, 490 (2011).
- [2] McIver, J. W., Hsieh, D., Steinberg, H., Jarillo-Herrero, P. & Gedik, N. Control over topological insulator photocurrents with light polarization. *Nature Nanotech.* **7**, 96 (2012).
- [3] Bergeret, F. S., Virtanen, P., Heikkila, T. T., & Cuevas, J. C. Theory of microwave-assisted supercurrent in quantum point contacts. *Phys. Rev. Lett.* **105**, 117001 (2010).
- [4] Palomaki, T. A., Harlow, J. W., Teufel, J. D., Simmonds, R. W. & Lehnert, K. W. Coherent state transfer between itinerant microwave fields and a mechanical oscillator. *Nature.* **495**, 210 (2013).
- [5] Bhadrachalam, P. et al. Energy-filtered cold electron transport at room temperature. *Nature Comms.* **5**, 4745 (2014).
- [6] Martínez-Pérez, M. J. & Giazotto, F. A quantum diffractor for thermal flux. *Nature Comms.* **5**, 3579 (2014).
- [7] Wyatt, A. F. G., Dmitriev, V. M., Moore, W. S. & Sheard, F. W. Microwave enhanced critical supercurrents in superconducting constricted Tin films. *Phys. Rev. Lett.* **16**, 1166 (1966).
- [8] Pals, J.A. & Dobben, J. Measurements of microwave-enhanced superconductivity in aluminum strips. *Phys. Rev. B* **20**, 935 (1979).
- [9] Tolpygo, S. K. & Tulin, V. A. Influence of microwave irradiation on high-frequency absorption by thin superconducting films (superconductivity stimulation). *Sov. Phys. JETP.* **57**, 123 (1983).
- [10] Heslinga, D. R. & Klapwijk, T. M. Enhancement of superconductivity far above the critical temperature in double-barrier tunnel junctions. *Phys. Rev. B* **47**, 5157 (1993).
- [11] Pals, J. A. & Dobben, J. Observation of Order-Parameter Enhancement by Microwave Irradiation in a Superconducting Aluminum Cylinder. *Phys. Rev. Lett.* **44**, 1143 (1980).
- [12] Entin-Wohlman, O. Comment on the observation of order-parameter enhancement by a change in the magnetic flux. *Phys. Rev. B* **23**, 2428 (1981).
- [13] Eliashberg, G.M. Film superconductivity stimulated by a high frequency field. *JETP Lett.* **11**, 114 (1970).
- [14] Beck, M. et al. Transient increase of the energy gap of superconducting NbN thin films excited by resonant narrow-band terahertz pulses. *Phys. Rev. Lett.* **110**, 267003 (2013).
- [15] de Visser, P. J. et al. Evidence of a nonequilibrium distribution of quasiparticles in the microwave response of a superconducting aluminum resonator. *Phys. Rev. Lett.* **112**, 047004 (2014).
- [16] Abrikosov, A. A. The magnetic properties of superconducting alloys. *J. Phys. Chem. Solids* **2**, 199 (1957).
- [17] Hartnoll, A., Herzog, C. P. & Horowitz, G. T., Building a Holographic Superconductor. *Phys. Rev. Lett.* **101**, 031601

(2008).

- [18] Montull, M., Pomarol, A. & Silva, P. J. Holographic Superconductor Vortices. *Phys. Rev. Lett.* **103**, 091601 (2009).
- [19] Maeda, K. & Okamura, T. Vortex flow for a holographic superconductor. *Phys. Rev. D* **83**, 066004 (2011).
- [20] Bao, N., Dong, X., Silverstein, E. & Torroba, G. Stimulated superconductivity at strong coupling. *JHEP* **10**, 123 (2011).
- [21] Natsuume, M. & Okamura, T. The enhanced holographic superconductor: is it possible? *JHEP* **08**, 139 (2013).
- [22] Gittleman, J. I. & Rosenblum, B., Radio-frequency resistance in the mixed state for subcritical currents. *Phys. Rev. Lett.* **16**, 734 (1966).
- [23] Marcon, R., Fastampa, R., Giura, M. & Silva, E. Vortex-motion dissipation in high- T_c superconductors at microwave frequencies. *Phys. Rev. B* **43**, 2940 (1991).
- [24] Golosovsky, M., Tsindlekht, M. & Davidov, D. High-frequency vortex dynamics in $YBa_2Cu_3O_7$. *Supercond. Sci. Technol.* **9** (1996).
- [25] Wördenweber, R., Hollmann, E., Schubert, J., Kutzner, R. & Panaitov, G. Flux transport in nanostructured high- T_c films at microwave frequencies. *Physica C* **479**, 69 (2012).
- [26] Blatter, G., Feigel'man, M. V., Geshkenbein, V. B., Larkin, A. I. & Vinokur, V. M. Vortices in high-temperature superconductors. *Rev. Mod. Phys.* **66**, 1125 (1994).
- [27] Clem, J. R. Local temperature-gradient contribution to flux-flow viscosity in superconductors. *Phys. Rev. Lett.* **20**, 735 (1968).
- [28] Shekhter, A., Bulaevskii, L. N. & Batista, C. D. Vortex viscosity in magnetic superconductors due to radiation of spin waves. *Phys. Rev. Lett.* **106**, 037001 (2011).
- [29] Gurevich, A. & Ciovati, G. Dynamics of vortex penetration, jumpwise instabilities, and nonlinear surface resistance of type-II superconductors in strong rf fields. *Phys. Rev. B* **77**, 104501 (2008).
- [30] Larkin, A. I. & Ovchinnikov, Y. N. Nonlinear conductivity of superconductors in the mixed state. *Sov. Phys. JETP.* **41**, 960 (1976).
- [31] Doettinger, S. G. et al. Electronic instability at high flux-flow velocities in high- T_c , superconducting films. *Phys. Rev. Lett.* **73**, 1691 (1994).
- [32] Buscaglia, G., Bolech, C. & López, A. On the numerical solution of the time-dependent Ginzburg-Landau equations in multiply connected domains. *Connectivity & Superconductivity*, J. Berger and J. Rubinstein (Eds.), Springer (2000).
- [33] Coffey, M. W. & Clem, J. R. Theory of rf magnetic permeability of isotropic type-II superconductors in a parallel field, *Phys. Rev. B* **45**, 9872 (1992).
- [34] Vodolazov, D. Y. & Peeters, F. M. Rearrangement of the vortex lattice due to instabilities of vortex flow. *Phys. Rev. B* **76**, 014521 (2007).
- [35] Silhanek, A. V. et al. Influence of artificial pinning on vortex lattice instability in superconducting films. *New Journal of Phys.* **14**, 053006 (2012).
- [36] Grimaldi, G., et al. Magnetic field and temperature dependence of the critical vortex velocity in type-II superconducting films. *J. Phys.: Condens. Matter* **21**, 254207 (2009).
- [37] Milosevic M. V., Peeters F. M., Commensurate vortex configurations in thin superconducting films nanostructured by square lattice of magnetic dots *Physica C* **404**, 246 (2004).
- [38] Gomez A., et al, Control of dissipation in superconducting films by magnetic stray fields *Appl. Phys. Lett.* **102**, 052601 (2013).
- [39] Aliev F. G., et al., Spin waves in circular soft magnetic dots at the crossover between vortex and single domain state *Phys.*

Rev. B **79**, 174433 (2009).

ACKNOWLEDGEMENTS

Authors gratefully acknowledge Yu. Galperin, T. M. Klapwijk and V. Vinokur for insightful discussions and A. Awad for experimental help on the initial stages. This work has been supported in parts by Spanish MINECO (MAT2012-32743), Comunidad de Madrid (NANOFRONTMAG-CM S2013/MIT-2850) and NANO-SC COST-Action MP-1201. A. Lara thanks UAM for FPI-UAM fellowship. Authors thank CCC-UAM (SVORTEX) for computational capabilities. The work of A.V.S. was partially supported by Mandat d'Impulsion Scientifique of the F.R.S.-FNRS.

Appendix A: Supplementary Material

Experimental details: The 60 nm thick Pb films were electron-beam evaporated onto liquid nitrogen-cooled Si/SiO₂ substrates. All samples were covered with a 20 nm thick protective layer of amorphous Ge, to avoid oxidation and keep them from getting scratched, since they are placed face down over the CPW. The Pb film is evaporated in all samples over a surface of 5×5 mm². In the Pb-PPC samples, the Pb films were deposited over a 2×2 mm² square array of 30 nm thick 1000 nm diameter Py dots, with an interdot distance of 2000 nm.

Hysteresis cycles confirmed that the Pb films are type II SC, in accordance with previous reports [1]. To reach the superconducting state, a JANIS helium cryostat with a superconducting magnet inside is used. Using two temperature control loops, the temperature stability is better than 0.2 mK and could be maintained up to 3 days.

The sample is placed at the end of an insert which contains a coplanar waveguide (CPW) to provide the microwave drive field (\mathbf{h}_{rf}) up to about 0.1 Oe parallel to the plane. Supplementary Fig. A.1 shows a calculation of the x and y components of the magnetic field generated near the central conductor, at a vertical distance of 20 nm for $P = 5$ dBm. The expressions found in [2] have been used for these calculations.

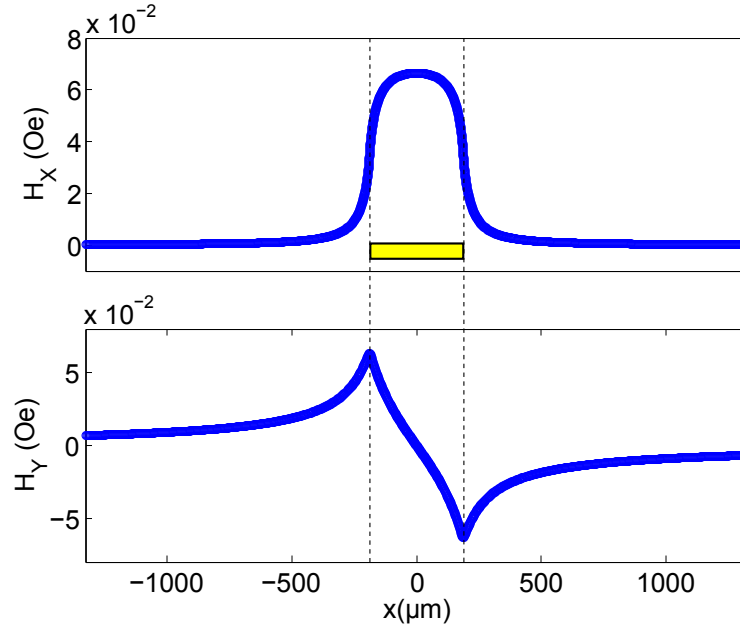


FIG. A.1. Magnetic field generated by the CPW at a vertical distance of 20 nm (sample surface) and $P = 5$ dBm. The yellow rectangle shows the dimensions of the central conductor of the CPW.

The CPW is designed to have a characteristic impedance of 50 Ω up to 25 GHz and emits mainly in the TEM mode. The central conductor is 375 μm wide, and the gap to ground planes is 140 μm . The CPW is made of Rogers laminates RO4350 10MIL/RO4003C 8MIL with a copper gladding (66 μm thick), and an extra gold plating on top. This waveguide does not excite the sample (placed on top of it) with a homogeneous field. Therefore, the vortices in different parts of the sample will feel a different amplitude and direction of the excitation. To account for how much vortices are excited on top of the central conductor, compared to far from it, in Suppl. Fig. A.2 we show a

histogram of the distribution of intensities of the microwave field. The largest value of field (corresponding to right in the middle of the central conductor) is found with a large frequency in the histogram, due to the almost parallel shape of the field close to this part of the waveguide. A large contribution can be seen in the histogram at low fields if long distances from the central conductor are considered in the calculations. With the appropriate weighting of each field with its frequency of appearance (inset of Fig. A.2), we find that at a field $H_x=0.034$ Oe (corresponding to the edge of the CPW), this weighted signal equals 17% of the maximum, which is achieved at the center of the CPW. Therefore, vortices lying on top of the central conductor will be excited by an 83% of the total field delivered by the waveguide. The rest of the excitation lies beyond the central conductor.

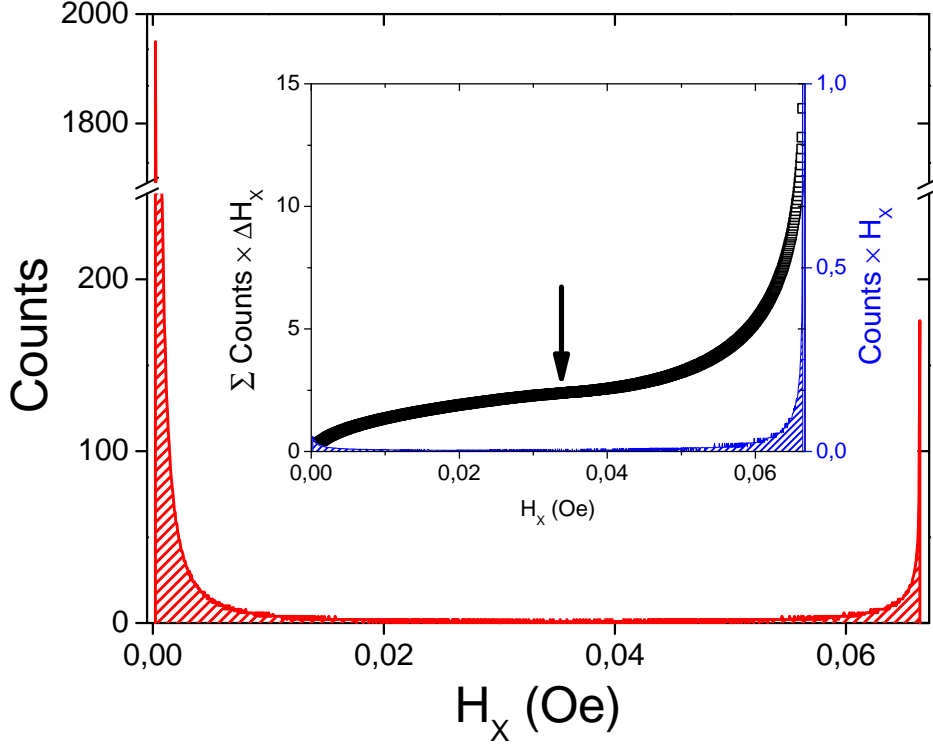


FIG. A.2. Histogram of distribution of magnetic microwave field created by the CPW. The inset shows a weighted distribution of fields (blue area) and a cumulative distribution. The arrow marks the field at the edge of the central conductor.

More details on this setup can be found in [3]. The high frequency signal is emitted from one port of the Vector Network Analyzer, VNA, (an Agilent E8363C PNA model was used, with frequency range up to 40 GHz and power up to 7 dBm) and propagates through the CPW, to finally reach the other port.

The VNA emits a signal of some known power, but due to reflections inside the high frequency cables (two 1.5 m long cables in the insert to carry the signal inside the cryostat, and two 0.6 m long cables to connect them to the VNA) and connectors, and their heating due to eddy currents, microwave power is not fully transmitted from one port of the VNA to the other. The value of the signal frequency (f) is related to the appearance of internal reflections, and a f sweep gives the information of how much power is transmitted at every frequency by means of the $S_{21}(f)$ parameter. The power of the signal at the CPW, that we refer to as P in the article, is estimated as the average of

the power emitted from port 1 and the power received at port 2, since the cables configuration connected to both ports is symmetric. We start from the definition of the transmission parameter in terms of voltages, when no signal comes out from port 2:

$$|S_{21}| = \left| \frac{V_{2,in}}{V_{1,out}} \right| \quad (\text{A1})$$

In this expression, $V_{2,in}$ refers to the voltage (amplitude and phase) of waves entering port 2, and $V_{1,out}$ to voltage of waves emitted from port 1. In terms of power, the expression for the amplitude is:

$$|S_{21}| = \sqrt{\frac{P_{2,in}}{P_{1,out}}} \quad (\text{A2})$$

Knowing $S_{21}(f)$, directly measured with the VNA, the power at port 2 is calculated as:

$$P_{2,in} = |S_{21}|^2 P_{1,out} \quad (\text{A3})$$

and the estimated power at the waveguide, P , is taken as the average:

$$P = \frac{P_{1,out} + P_{2,in}}{2} = P_{1,out} \frac{(1 + |S_{21}|^2)}{2} \quad (\text{A4})$$

It is to be noted that this P does not refer to the radiated electromagnetic energy incident on the sample, just to the power associated to the current that produces this radiation, as it propagates through the CPW.

This correction helps to quantify the losses due to the relation between wavelength and length of the cables. Higher frequency signals suffer more reflections, and are not so well transmitted to the second port, which can be quantified via S_{21} . However, more factors can contribute to decrease the power that is delivered to the sample, such as not perfectly symmetric cables, that would decrease the accuracy of the previous average. Also, it is important to remember that working at low temperatures can result in important differences compared to room temperature, due to changes in the length of cables, etc. In our case, this is not a problem, since the range of variation of T is small, always very close to T_c . Also, even if we could take into account all losses, the results presented in the main text are relative (throughout the range of powers considered, where transmission efficiency is invariant, since the frequency is fixed), and a correction of the absolute value of power will not affect the presence of the observed effects.

Measurement of the permeability parameter U : For the data analysis (i.e. calculation of the real and imaginary parts of U) the reflected signal is neglected (S_{11} coefficient of VNA), since its relative variation with respect to a reference trace is more than 15 times lower in magnitude than the transmitted signal (S_{21} coefficient). The same increase of T_c^* and H_{c2}^* at intermediate powers has been observed on the reflection coefficient S_{11} alone as well.

The permeability parameter was analyzed as the VNA transmission parameter (S_{21}) for every field normalized by the same parameter corresponding to the normal state of the sample, similar to the analysis method used in [4]:

$$\mu \propto U(f, P, H) = \frac{S_{21}(f, P, H)}{S_{21}(f, P, H_{\text{ref}})} \quad (\text{A5})$$

Here $S_{21}(f, P, H)$ and $S_{21}(f, P, H_{\text{ref}})$ are the (f) and (P) dependent forward transmission parameters at the applied field of interest H , and the reference field H_{ref} (the maximum applied field, higher than H_{c2}). This expression is used when T is kept constant and H is changed. An analogous analysis is used in T sweeps at constant H , but normalizing at a reference temperature. It is necessary to achieve the normal state, either by increasing T or H , to have a clear signal corresponding to the SC response, when compared with the normal response, so well above T_c or H_{c2} conditions are necessary for a correct normalization. The quantity U is complex, and the imaginary part of $U = U' + iU''$, U'' , represents microwave losses, while the real part U' represents energy stored and exchanged between sample and circuit (CPW), in this case flux screening by the superconductor.

Once U is found, values of T_c and H_{c2} can be found when reaching high enough values of T or H , so that the region in which the sample is in the normal state is clearly differentiated from the superconducting region. Since the transition is not perfectly sharp and well defined, the following method to determine T_c and H_{c2} will be used. To our best knowledge, there is not a universal criterion for extracting from permeability data the critical values of field and temperature. Therefore, in the following we will refer to the critical values obtained as T_c^* and H_{c2}^* , that may not be the exact values of critical T and H , but from which a clear dependence with microwave power is observed, that we interpret as stimulation of superconductivity by microwaves.

T_c^* is extracted from T sweeps at constant f and H , but varying P , so that MSSC can also be detected in these measurements. On the other hand, H_{c2}^* is found from H sweeps in which T and f are kept constant, while P also changes, to evidence the presence of MSSC not only from the values of T_c^* , but also from H_{c2}^* . For the results of T_c^* and H_{c2}^* discussed in this article, the real part of U was used, only because its changes are larger and easier to observe and analyze, but the superconducting transition is equally visible in U' and U'' .

Critical temperature: The values of T_c^* were found in T sweeps by finding the intersection between piecewise polynomial fit of the response in temperatures for each power in both the superconducting part, and the normal part (see Suppl. Fig. A.3 for an example of a T sweep at $f = 6$ GHz and $P = -17$ dBm, corresponding to Fig. 1c in the article). The resulting dependence of T_c^* on power clearly shows an increase at intermediate values of power. Analogous results (increase of T_c at intermediate powers) are also achieved when directly plotting the temperature at which the response changes in a (for example) 1% with respect to the normal state. The error in T_c^* , of 1 mK, is obtained statistically as the dispersion in the intersection, found by least squares.

Critical field: From measurements of $U(f, P, H)$ similar to those shown in Fig. 2a of the article (H sweeps) one can determine H_{c2}^* as the borderline separating the normal region from the superconducting one. As can be seen in Suppl. Fig. A.4, showing a typical magnetic field dependence of $U'(f, P, H)$ at $P = -15$ dBm, $T = 7.17$ K and $f = 6$ GHz while changing the applied field, the transition from normal to superconducting state is not completely abrupt (the same happens when finding T_c^*). We define H_{c2}^* as the intersection of the polynomial low field fit of $U'(f, P, H)$ shown by a red solid line and the high field level corresponding to the normal state and fitted by blue lines.

The value of critical field for each microwave power is considered as the average of the values obtained for positive and negative fields, to cancel the shift produced by the magnetic field frozen in the superconducting magnet.

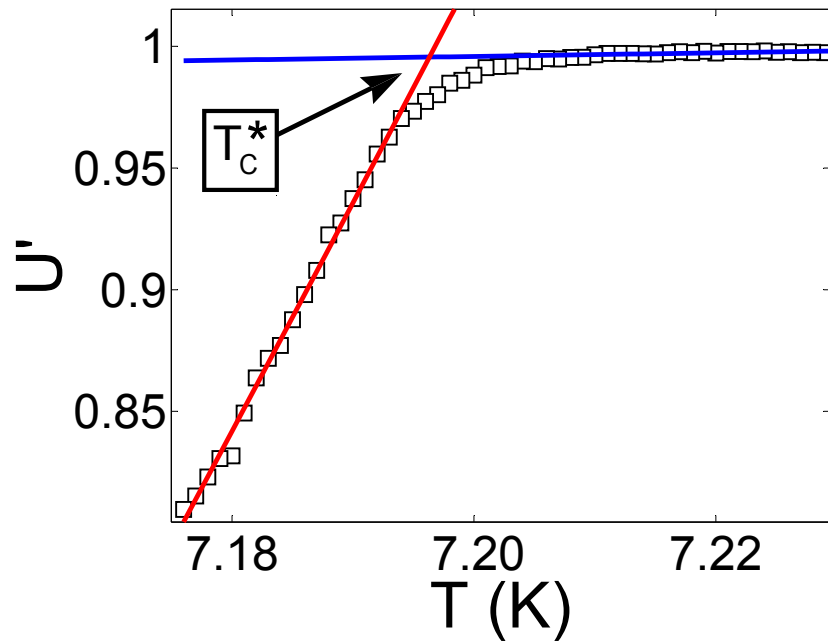


FIG. A.3. Method to determine T_c . In this case, U' is considered.

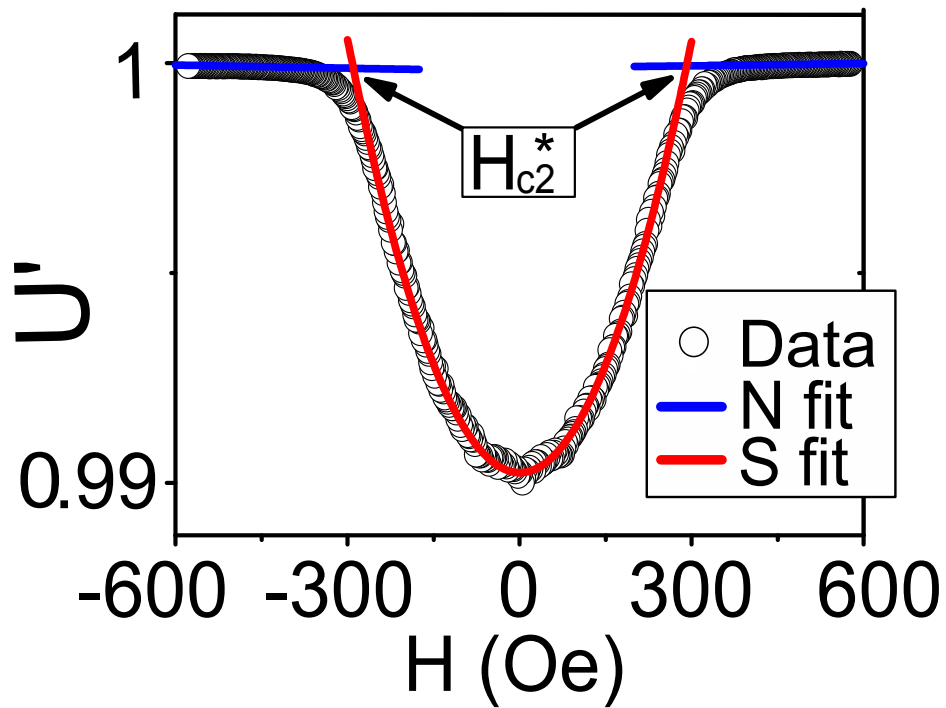


FIG. A.4. Method to determine H_{c2}^*

Analogous results (increase of H_{c2}^* at intermediate powers) are also achieved when directly plotting the field at which the response changes in a (for example) 0.01% with respect to the normal state.

Additional results and discussion:

Range of power considered: The VNA that we used can sweep power down to -40 dBm. We show results from -27 to 7 dBm. At powers lower than -27 dBm the sensitivity starts to decay rapidly, and there is noise that does not allow to have clear results. Also, a change of range is at -27 dBm, and some discontinuities may appear in the response. Despite the noise, the tendency at lower powers (not shown) is to present a constant signal (no changes of P_O are observed in that region).

Influence of pinning: The article deals mainly with the sample with PPCs, since the stimulation of superconductivity appears to be stronger than in plain films. As a comparison, the same analysis presented in Fig. 2c in the article is shown in Suppl. Fig. A.5 for the plain Pb film. It can be noted that the maximum relative upper critical field is lower in the plain films in comparison with Pb-PPC films. The introduction of pinning in Pb-PPC therefore seems to enhance the MSSC-related increase of H_{c2}^* . The experimentally observed stronger (and in a wider temperature interval) effects in the films with artificial vortex pinning could be linked with pairbreaking effects [5] from the Py dots stray fields [6]

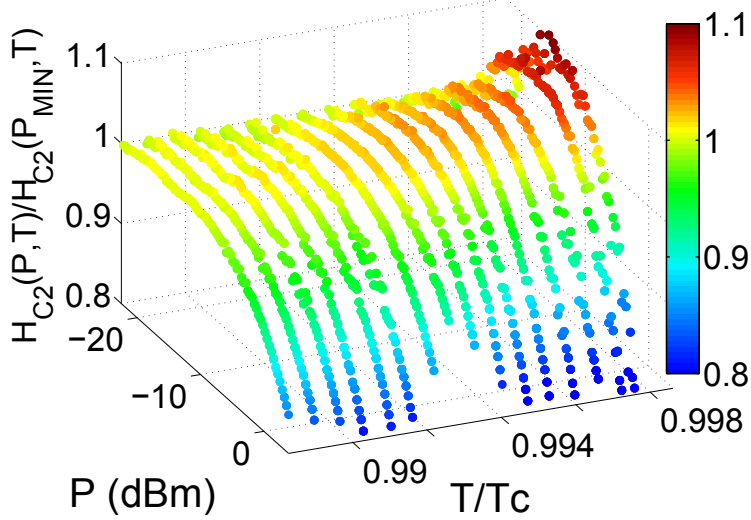


FIG. A.5. Relative critical field in the plain 60 nm thick Pb film

P_O close to H_{c2}^ far from T_c :* Concerning the dependence of P_O on H , as explained in the article, it increases when increasing H . Close to T_c this trend is uniform, but at lower temperatures, and higher fields local maxima in optimum power appear (see Suppl. Fig. A.6), as mentioned in the article, but not shown in Fig. 3b. We explain this behavior as a consequence of a dense vortex structure, when vortices are not able to move as freely as in cases with less density of them, diminishing the LO effect.

Anomalies in dissipation at matching fields: At frequencies below 2 GHz it is observed that matching anomalies transform from maxima to minima depending on f and P , at $T = 7.1$ K, as shown in Fig. 3 c) and Supplementary Fig. A.7 in the article.

In Figs. 3b and 3c in the main text and in Supplementary figures A.6 and A.7, matching fields have been indicated (*a posteriori*) with dotted lines. From these values we can verificate the interdot separation of the dots comprising the array of PPCs, as follows:

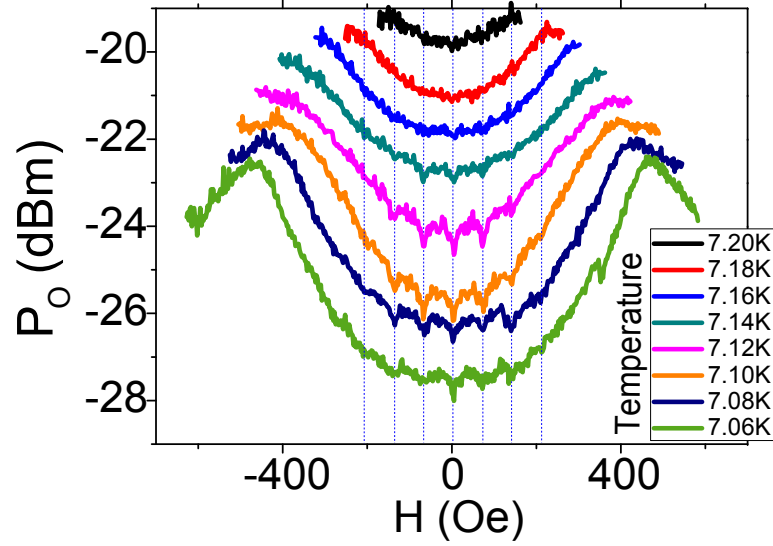


FIG. A.6. Optimum power as a function of magnetic field in the Pb-PCC film

$$H_{\perp} = \frac{\phi_0}{a^2} \rightarrow a = \sqrt{\frac{\phi_0}{H_{\perp}}}$$

Our measurements in the case of field perpendicular to the film (Supplementary Fig. A.8) give a value of matching fields of 4.8 Oe. With the standard value of the flux quantum, $\phi_0 = 2.06783 \cdot 10^{-15}$ Wb. Then, the interdot distance is, as expected:

$$a = \sqrt{\frac{\phi_0}{H_{\perp}}} = 2.075 \mu m \simeq 2 \mu m$$

Mainly the out of plane component creates the vortices that will give raise to matching conditions. Then, we can estimate the inclination of the field from the matching conditions. We know that matching fields for a perpendicular field occur at 4.8 Oe. Then, if we measure them at 72 Oe in the inclined configuration, as in Fig. 3b and 3c in the main text, we can extract the inclination angle as its sine, which equals the ratio of both quantities: $\sin \alpha = \frac{4.8}{72} = 0.066 \rightarrow \alpha = 3.78^\circ$

Dependence of the superconductivity stimulation on the magnetic field direction: Let us first discuss possible reasons why MSSC in the type II superconductors could be more clearly observed in an inclined magnetic field. We explain this observation as follows: As long as the applied microwave frequencies are substantially less than corresponding to the zero temperature gap values ($f_{Pb}(T = 0K) = 653$ GHz), and microwaves interact only with normal quasiparticles, the effectiveness of MSSC is conditioned by the presence of low energy normal quasiparticle states [7]. An additional (in-plane) external magnetic field effectively suppresses the order parameter, creating a gapless state in a rather extended field interval $\frac{H_{c2}}{2} < H < H_{c2}$ [5]. Then, for the suppressed order parameter values (i.e., close to T_c) the quasiparticles DOS varies roughly as \sqrt{E} (here E is measured from the center of the gap) in the presence of impurities,

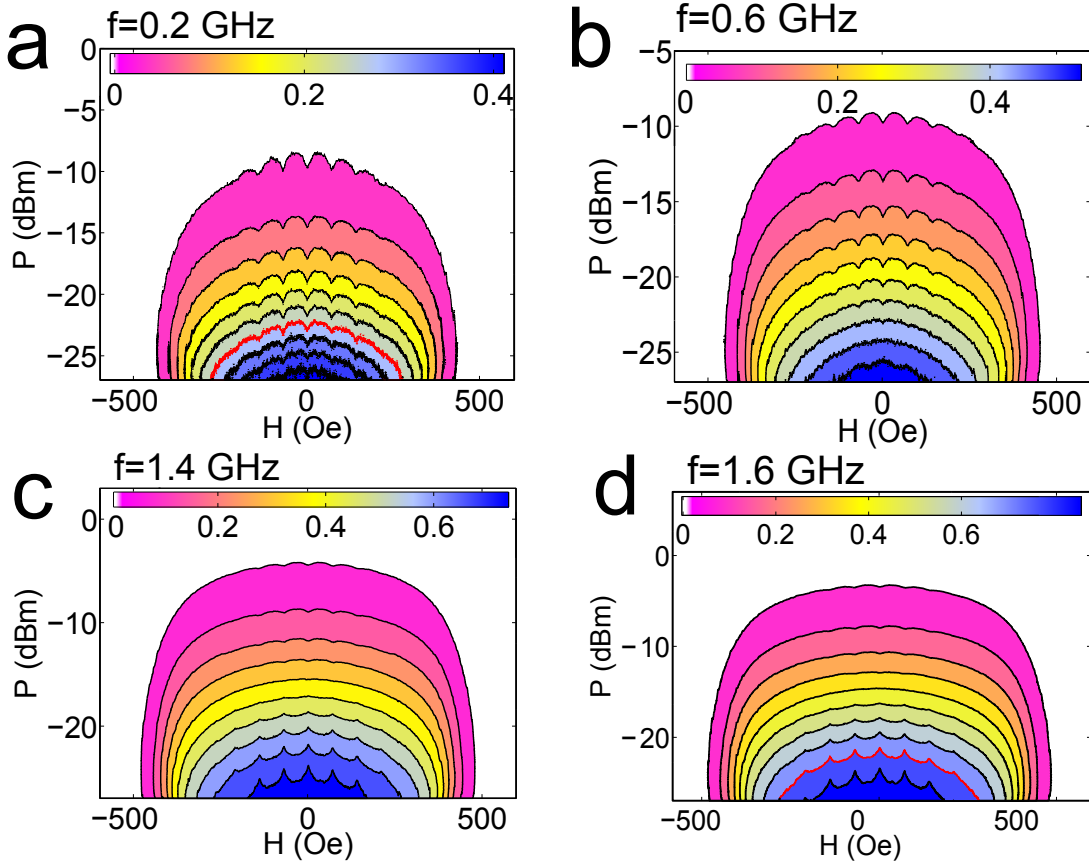


FIG. A.7. U'' as a function of H and P at different frequencies around 1 GHz. Panels a) and d) highlight a contour in red to stress the change from peaks to dips with frequency.

providing effective quasiparticle excitation by subgap (GHz) microwaves [5]. Our experimental observations (Suppl. Fig. A.6) reveal a clear enhancement of the MSSC strength in the form of an increase of P_O in the field interval ($\frac{H_{c2}}{3} < H < \frac{3}{5}H_{c2}$) followed by some small suppression of the P_O above $\frac{3}{5}H_{c2}$. Within our model, this increase is related in parts with an increase of the low energy quasiparticles DOS in the indicated field interval (mainly from in-plane field component) and enhanced contribution of the LO effects (from perpendicular field component) while vortex-vortex interaction remains unimportant.

It could be argued that the in-plane component of the inclined field can produce changes in the stray field of the dots, that would in turn affect the behavior of vortices. Experimental data of the dots shows that their annihilation field is higher than the values we work with in this case, so the stray field is always kept to a minimum. Direct measurements of U'' comparing the case of perpendicular and inclined field confirm that matching fields fall in the same values (obviously, after correspondingly scaling the fields, to match the perpendicular to the plane components, Supplementary Fig. A.8)

Time dependent Ginzburg Landau simulations:

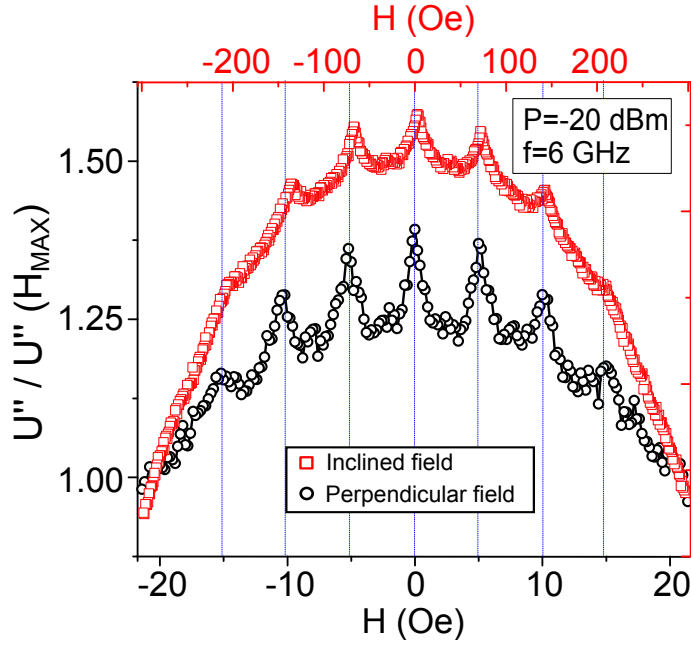


FIG. A.8. Comparison of matching fields in the case of perpendicular and inclined field.

In order to understand the behavior of vortices under an in plane ac magnetic field, we have developed a computer program to simulate the 3D time dependent Ginzburg Landau (TDGL) equation. The equations can be expressed in a dimensionless form as follows [8]:

$$\frac{\partial \Psi}{\partial t} = -\frac{1}{\eta} \left[\left(-i\vec{\nabla} - \vec{A} \right)^2 \Psi + (1 - T) \left(|\Psi|^2 - 1 \right) \Psi \right] \quad (\text{A6})$$

$$\frac{\partial \vec{A}}{\partial t} = (1 - T) \text{Re} \left\{ \Psi^* \left(-i\vec{\nabla} - \vec{A} \right) \Psi \right\} - \kappa^2 \vec{\nabla} \times \vec{\nabla} \times \vec{A} \quad (\text{A7})$$

Where Ψ is the order parameter, \vec{A} the vector potential and η a constant relating the relaxation times of normal and superconducting electrons. We use a finite difference scheme, a 2D version of which has been extensively used in the past. However, the more complicated geometry we want to reproduce cannot be achieved in 2D, since magnetic flux (used for boundary conditions) needs at least two layers to be accommodated in the simulated domain (flux enters through a surface, therefore a single layer in 2D is not enough for considering in plane component of the magnetic flux, just perpendicular to the plane).

The equations integrated in time are four, one for the order parameter (first Ginzburg Landau equation), and the other three for the auxiliary variables known as link variables (see [8] for more details), that can be obtained by rearranging the three components of the second Ginzburg Landau equation for the vector potential. Link variables are defined as:

$$U_{x,y,z}^x = e^{-i \int_{x_0}^x A_x(\xi,y,z,t) d\xi}$$

$$U_{x,y,z}^y = e^{-i \int_{y_0}^y A_y(x,\eta,z,t) d\eta}$$

$$U_{x,y,z}^z = e^{-i \int_{z_0}^z A_z(x,y,\zeta,t) d\zeta}$$

Where x_0 , y_0 and z_0 are arbitrary points of space that eventually cancel out. Given a plane, XY for example, the rectangle formed by the cells in (i, j) , $(i+1, j)$, $(i, j+1)$ and $(i+1, j+1)$ will hold a circulation of the vector potential that can be related to magnetic flux at that position inside the superconductor:

$$\oint_{\partial\Sigma} \vec{A} \cdot d\vec{l} = \iint_{\Sigma} \vec{B} \cdot d\vec{s} = \Phi_B$$

From such a rectangle the discretized distribution of magnetic field can be found in the $x = i$, $y = j$, $z = k$ coordinates:

$$U_{i,j,k}^x U_{i+1,j,k}^y \overline{U}_{i,j+1,k}^x \overline{U}_{i,j,k}^y = e^{-iB(i,j,k)\Delta x\Delta y}$$

and a similar calculation for the other two planes YZ and ZX .

The geometry that we simulate is that of a thin film, with four cells in vertical direction. Doing so, magnetic flux is imposed according to boundary conditions (continuity of the parallel component of H) in the top and bottom planes, and allowed to evolve according to TDGL in the center of the film. The in plane dimensions are of $25\xi \times 25\xi \times 3\xi$, being ξ the coherence length, that is the unit of length of the simulations (its absolute value is not specified, it enters the computations through the Ginzburg Landau κ parameter). This is enough to distinguish clearly vortices from each other and from the borders, and at the same time small enough to allow for relatively fast computations. This is so because 3D version of TDGL needs to consider terms that 2D does not, since there are more types of possible border cells, making it inevitably slower to calculate than just N times slower, being N the number of cells in vertical direction. Details about the discretization of TDGL equations for a rectangular mesh can be found in [8].

By choosing an appropriate value of $\kappa = 2$, vortices appear when applying a perpendicular to the plane magnetic field above H_{c1} . This field is applied until the vortex lattice is stationary (vortices enter from the borders towards the center). Then, the ac magnetic field is applied parallel to the plane (keeping unchanged the perpendicular DC field). Keeping track of macroscopic quantities (such as the total magnetization) we can extract information about the global response of the system (vortices and the rest of the system, including borders), such as difference of phase with respect to external signal (for very high frequencies, vortices start to not being able to follow the field). However, we are more interested in the ‘‘microscopic’’ behavior of vortices, that can be studied by looking directly in the values of $|\Psi|$ at each simulation cell.

It has been found that vortices shape and position as a function of time depend both on frequency and amplitude of the external ac field. In general, under an in plane ac field vortices have been found to periodically shrink and widen in size (See Figure 4 in the main text). If microwave power (amplitude of the ac field) is large enough, these oscillations are seen very clearly. In Fig. 4d of the main text we show the variation in vortex core radius Δr at a fixed value of $|\Psi| = 0.5$ as a function of frequency for different powers. Higher powers allow to see better this difference, that is always present. The higher the difference of phase between ac field, and dynamic magnetization is, the more

difficult is for the vortex to follow the external excitation, and these oscillations are not so well observed. As for the average radius of the vortex core, at higher frequencies it decreases, as predicted by LO, due to a redistribution of quasiparticles outside the vortex core.

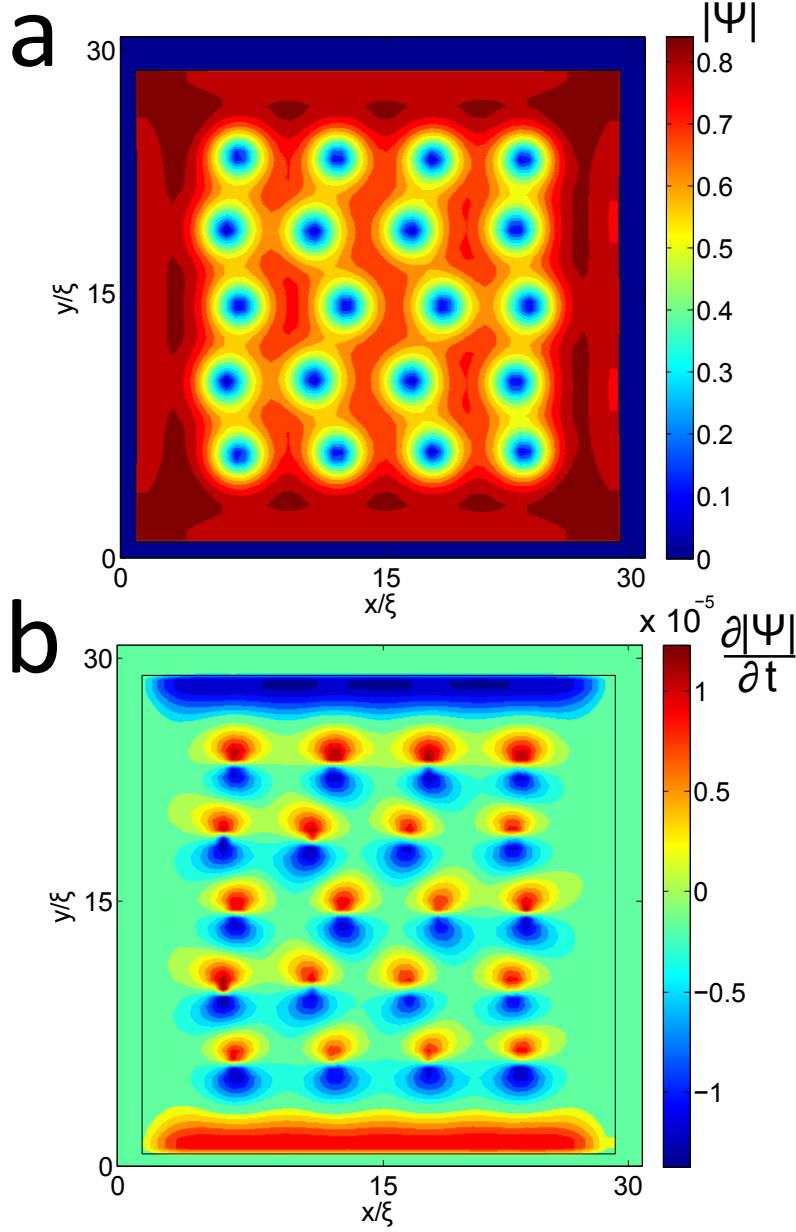


FIG. A.9. a) Magnitude of the order parameter for $H_{DC} = 0.4H_{c2}$. b) Time derivative of panel a). Vortices move toward the blue area. Half a period later, colors interchange

It is to be noted that in solving TDGL equations, no energetic considerations for stability of Cooper pairs is made, therefore effects such as Cooper pairs breaking due to absorption of photons of energy above the superconducting gap are not found. An arbitrarily high frequency ac field just makes it harder for vortices to follow it, not being frequency a cause of loss of superconductivity. On the other hand, a higher amplitude of the ac field does indeed

destroy superconductivity. For example, at $|\mathbf{h}_{\text{rf}}| = H_{c1}$, $|\Psi| < 1$ far from vortices. Thus, not only vortices are affected by large amplitude ac fields, also the rest of the film (as was already discussed before, concerning the excess of normal quasiparticles (unpaired electrons) when applying an inclined DC field).

It is important to note that in TDGL equations, there is no notion of Cooper pair, neither of their bonding energy. Typically, photons of energy in the THz range are energetic enough to break a Cooper pair when being absorbed by them, since this energy corresponds to the superconducting gap energy $\Delta \sim \text{meV}$. Therefore, even when we apply an ac field of frequencies the order of THz, the order parameter is not going to drop to zero because we are reaching the frequency corresponding to the superconducting gap. This concept is not considered in the equations we are solving. TDGL equations are useful for our purpose in that they give information on the redistribution of normal quasiparticles by applying an ac field to the vortex lattice, just by the deformation and movement of vortex cores. This redistribution of normal quasiparticles further interacts with the electromagnetic radiation of the waveguide, and create extra losses due to Joule heating.

Influence of defects In the simulations, no periodic pinning centers are considered, we use them to study the reaction of vortices to a high frequency magnetic field.

However, the presence of defects can be considered. They are introduced by replacing the term $(|\Psi|^2 - 1)$ by $(|\Psi|^2 - r)$ (see [8]). Here, the term r is a variable that depends on position, and ranges between 1 and 0. By choosing values of r lower than 1, the superconductivity is weaker at those points, and vortices are in a more stable position, so it acts as a pinning center for vortices. In simulations we have used a defect of size ξ , with $r=0$ to trap a vortex. Several simulations at different frequencies show that regardless a vortex is inside a defect or not, the core size oscillates, as described in the main text. However, displacements of the vortex core are different, being more able to follow the external field when trapped. The vortices outside the defects also move but, especially at low frequencies, they tend to move in more circular trajectories, unlike vortices trapped in defects, which move more linearly. Also, radial oscillations of the vortex core size are observed both for vortices trapped inside defects, or outside defects, with a somewhat larger difference in amplitude at lower frequencies, as shown in Supplementary Fig. A.10.

-
- [1] Dolan, G. J. and Silcox, J. Critical Thicknesses in Superconducting Thin Films. *Phys. Rev. Lett.*, **30**, 603 (1973).
 - [2] Chumakov, D. et al. Nanosecond time-scale switching of permalloy thin film elements studied by wide-field time-resolved Kerr microscopy. *Phys. Rev. B* **71**, 014410 (2005)
 - [3] Awad, A. A. et al. Flux avalanches triggered by microwave depinning of magnetic vortices in Pb superconducting films. *Phys. Rev. B* **84**, 224511 (2011)
 - [4] Kuanr, B. K., Camley, R. E. and Celinski, Z. Extrinsic contribution to Gilbert damping in sputtered NiFe films by ferromagnetic resonance. *J. Magn. Magn. Mat* **286**, 276-281 (2005)
 - [5] Dukan, S. and Tesanovic, Z., Density of states of a type-II superconductor in a high magnetic field: Impurity effects. *Phys. Rev. B* **56**, 838 (1997).
 - [6] Lange, M., Van Bael, M. J., Bruynseraede, Y. and Moshchalkov, V. V. Nanoengineered magnetic-field-induced superconductivity. *Phys. Rev. Lett.*, **90**, 197006 (2003).

- [7] Eliashberg, G. M. Film superconductivity stimulated by a high frequency field. *JETP Lett.* **11**, 114-116 (1970).
- [8] Buscaglia, G., Bolech, C. and López, A. On the numerical solution of the time-dependent Ginzburg-Landau equations in multiply connected domains. *Connectivity & Superconductivity*, J. Berger and J. Rubinstein (Eds.), Springer (2000)

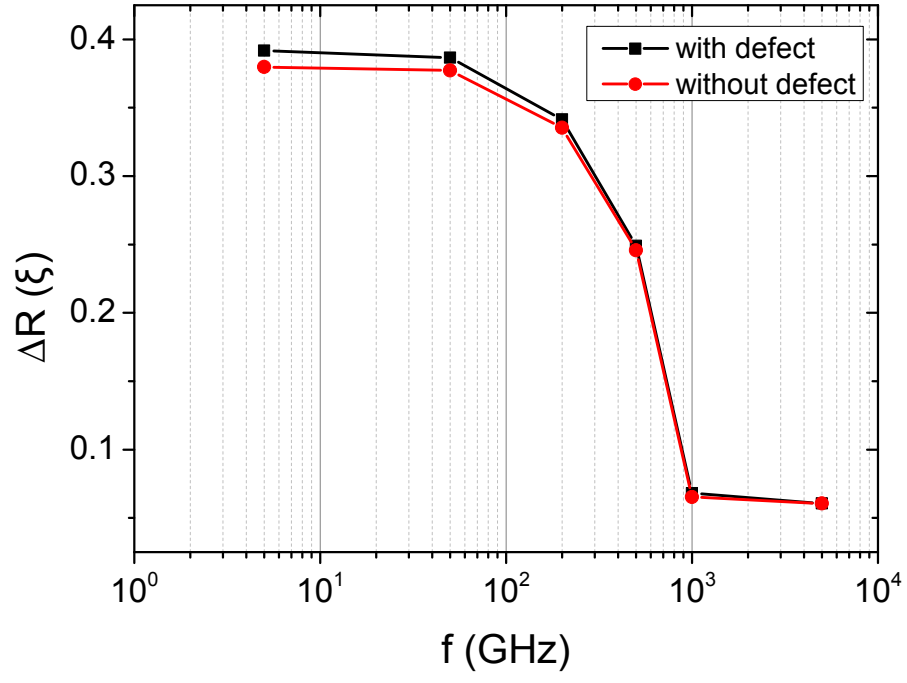


FIG. A.10. Frequency dependence of radial oscillations magnitude for a vortex trapped in a defect, or outside of it.